



The SFIR Test: An Innovative Hydrostatic Compression Test to Characterize the Volumetric Behavior of Polymeric Foams

J. Becker^{1,2} · M. Le Saux¹ · P. Charrier² · W. Hervouet² · V. Le Saux¹ · L. Maheo^{3,4} · Y. Marco¹

Received: 6 March 2024 / Accepted: 12 July 2024
© Society for Experimental Mechanics 2024

Abstract

Background Polymeric foam materials can show a strongly non linear compressible elastic response. For certain applications, it is necessary to know the volumetric behavior of the material under hydrostatic compression. Existing devices for hydrostatic compression testing use a multiaxial testing machine or a fluid to transmit pressure to the foam. They are either complex to set up, or do not allow for hydrostatic pressures of several MPa to be applied or for volume variations of several tens of percent to be achieved. Besides, when pressure is applied to the sample via a fluid, it is difficult to prevent penetration of the fluid into the foam, particularly when it is open-cell.

Objective This paper presents a hydrostatic compression test for polymeric foams that does not present these limitations.

Methods A cylinder of a nearly incompressible material (silicone) is molded around a spherical sample of the polymeric foam of interest. The whole set is subjected to confined compression in a rigid chamber. Post-processing is developed, based on finite element analysis, to determine the hydrostatic stress in the foam and its volume ratio from the axial load and displacement data.

Results Finite element simulations show that the foam sample is subjected to a state close to hydrostatic compression. The test was applied to several samples of elastomeric microcellular polyurethane foams of different densities. The results are in line with expectations, with limited scattering.

Conclusions The Sphere Foam In Rubber (SFIR) test allows to reach volume reductions of several tens of percents and hydrostatic stress levels of several MPa, on any kind of polymeric foams, provided that its bulk modulus is at least 100 times lower than that of the surrounding nearly incompressible material used. It can be easily implemented with very standard equipment.

Keywords Polymeric foam · Hydrostatic compression test · Compressibility · Experimental

Introduction

Polymeric foams are today widely used in the industry thanks to their interesting load mitigating properties and their low density. In some applications, such as automotive jounce bumpers, these foams are subjected to multiaxial

compression-dominated mechanical loadings leading to very high volume reductions (up to 70%). In order to design such parts, the material mechanical response must be obtained under mechanical conditions consistent with those experienced by the material in service. This paper focuses on the response of the material under hydrostatic compression.

Literature reports hydrostatic compression tests for many materials [1], including rock, glass [2], soil [3], ice [4], metallic foam [5], rubber [6], and polymeric foams [7–14]. These tests can be classified in five categories. The first one, often called triaxial compression tests, consists in applying the pressure to each face of the specimen (a rectangular prism, a cube or a cylinder) using pistons on a multiaxial testing machine [15]. A second test category uses a gas to transmit the pressure to the sample, e.g., helium [16], air [8] or nitrogen [2, 9]: the sample is placed into a chamber connected to a compressor to increase the gas pressure.

✉ M. Le Saux
matthieu.le_saux@ensta-bretagne.fr

¹ ENSTA Bretagne, IRDL, UMR CNRS 6027, Brest 29200, France

² ESM department, Vibracoustic, Carquefou 44474, France

³ Université Bretagne Sud, IRDL, UMR CNRS 6027, Lorient 56100, France

⁴ Military Academy of Saint-Cyr Coetquidan, CReC Saint-Cyr, Guer 56380, France

In the third category, pressure is applied via a liquid, e.g., water [10, 17], oil [11], alcohol [7] or mercury (by adapting a porosimeter) [18]: the sample is placed in a chamber filled with a liquid whose pressure is increased by moving a piston. A fourth test category combines a confining pressure applied by a liquid and a compressive load applied in one direction using a piston [4, 5, 12]. A last test category consists in carrying out a confined compression test: a specimen, usually cylindrical, is compressed axially in a rigid chamber [19]. This last test is usually approximated as a hydrostatic compression test for nearly incompressible materials such as bulk elastomers.

In this study, the objective is to develop a hydrostatic compression test for polymeric foams, with the following constraints:

- easy to set up so that it can be used in most laboratories and industries with low security restrictions and standard equipment;
- allowing the strain and stress in the material to be evaluated;
- able to achieve pressures of at least 15 MPa so that it can be applied to relatively dense foams;
- suitable for materials whose volume can be reduced by 70% (volume ratio of 0.3) so that the foams of interest here can be deformed up to the densification phase (i.e., when the majority of cells are closed);
- with no exchange of fluid between the outside and the inside of the sample, for both closed-cell and open-cell foams.

The triaxial compression test often needs complex equipments with a multiaxial testing machine. It is not very well adapted for a highly deformable material. The hydrostatic tests using gas to transmit the pressure to the sample need a high pressure pump connected to a tank. This type of system poses sealing and safety issues. The pressure reached with these systems is usually not very high (e.g., 0.7 MPa for [8]) and thus are only suited for low density foams. Furthermore, they are not suitable for open-cell foams. The pressure achieved with systems using liquids to apply the pressure can be several MPa (e.g., 8 MPa for [13]), or even several tens of MPa (e.g., 80 MPa for [20]). However, applying such pressures to a liquid brings sealing issues and strict safety standards (risk of explosion) must be used. Moreover, open-cell foams specimens must be coated before the test [14, 21]. The confined compression tests can be considered as hydrostatic only for nearly incompressible material [19], which is not the case of foams.

Thus, none of the tests proposed in the literature fully meets the specifications mentioned above. The objective of this paper is to present a new hydrostatic compression test that meets these specifications. This test uses a solid to transmit the pressure to the specimen. A cylinder of a nearly incompressible elastomer is molded around the polymeric foam specimen and the set is put in confined compression in a chamber supposed

to be infinitely rigid (Fig. 1). Therefore, this test does not cause any sealing issues, does not need any complex apparatus and can easily reach high pressure levels. As shown in the present paper, a specific post processing of the experimental data, defined on the basis of finite element analysis (FEA) simulations, makes it possible to determine the pressure and the volume ratio of the foam specimen from only the global load and displacement data measured during the test.

The procedures used are presented in section “[Procedures](#)”. Section “[Post-processing Procedure](#)” describes the post-treatment applied to determine the foam sample volume ratio and the pressure inside it. The validity of the test and the proposed post-processing are discussed in section “[Validation of the Test and the Post-processing](#)”. Finally, section “[Results and Discussion](#)” presents the results obtained using this test and discusses reproducibility and sensitivity.

Procedures

Material and Samples

The material studied in this paper is a naphthalene diisocyanate-based cast elastomeric microcellular polyurethane (MCU), with closed cells, typical of those used for automotive jounce bumpers. The cells have been characterized in [22]. They are almost spherical with an average diameter of a few tenths of micrometres. Additionally, they are randomly distributed in space. This pleads for an isotropic macroscopic behavior. To promote homogeneous deformation of the foam specimen, spherical samples are used. A sphere is less easy to obtain than for another geometry, such

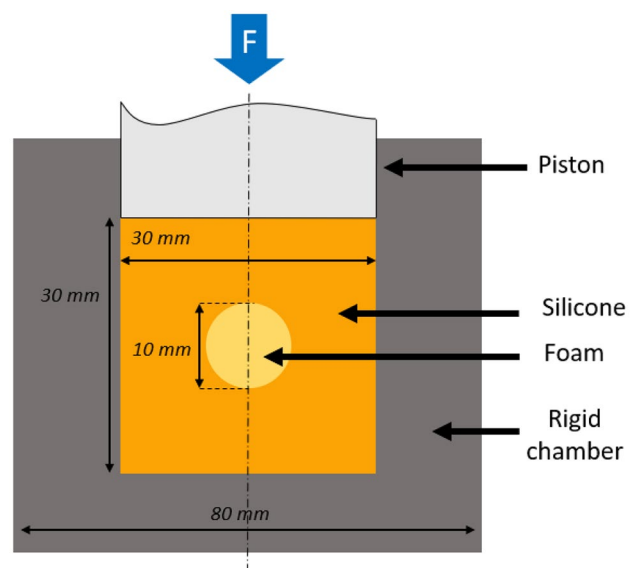


Fig. 1 Scheme of a section of the axisymmetric experimental setup

as a cylinder for example, but numerical simulations proved that this shape is required to obtain a stress state close to hydrostatic pressure up to large strain levels. The density of the samples is determined (with an uncertainty of about $20 \text{ kg}\cdot\text{m}^{-3}$) from measurements of their mass and dimensions. Samples with different densities ranging from $350 \text{ kg}\cdot\text{m}^{-3}$ to $560 \text{ kg}\cdot\text{m}^{-3}$ are used. The nearly incompressible elastomer used as a medium is a silicone from Aquasil® Ultra XLV, with a bulk modulus of 1430 MPa (measured from a confined compression test, as described below).

A silicone cylinder of 30 mm in height and 30 mm in diameter is used to meet the capacity (25 kN) of the machine used. Concerning the size of the foam, there are two limiting cases: if the foam sample is too small regarding the size of the silicone cylinder, the contribution of the foam response to the whole response of the [foam+silicone] sample is hard to detect. If the foam sample is too large (i.e., too close to the chamber), the foam does not deform homogeneously and is not subjected to hydrostatic compression, as confirmed by FEA. In addition, the size of the sphere must be larger than the representative elementary volume for the measured response to be statistically representative of the average response. A previous study [22], carried out on the same materials, has shown that the geometrically representative elementary volume is less than or equal to about 10 mm^3 . The relative size of the sphere and the chamber has been determined to achieve a good balance between sensitivity to the foam response and to keep a satisfying hydrostatic state (no walls effect). A sphere diameter of 10 mm was selected.

Sample Elaboration Protocol

The spherical foam samples (Fig. 2) are obtained by abrading a piece of foam to the desired diameter. The samples are then weighted with an accuracy of 1 mg and their average diameter is measured with a calliper with an accuracy of $\pm 0.1 \text{ mm}$. The next step is to ensure that the foam sample is well centered in the silicone cylinder. The molding procedure is depicted in Fig. 3(a). It consists of the three following main steps:

1. The foam sphere is fixed with a small needle in the center (1-3 in Fig. 3(a)). Then, the silicone is poured to mid-height (4 in Fig. 3(a)).
2. Ten min later, the needle is removed from the foam (5-7 in Fig. 3(a)) and the other half of the silicone is poured (8 in Fig. 3(a)).
3. After curing of the silicone, the cylinder is cut to the desired height (9 in Fig. 3(a)).

The silicone is not absorbed by the foam, thanks to the closed cells microstructure. The surface is not coated and the silicone penetration is limited to the cells intersected by the external surface.



Fig. 2 Foam sample

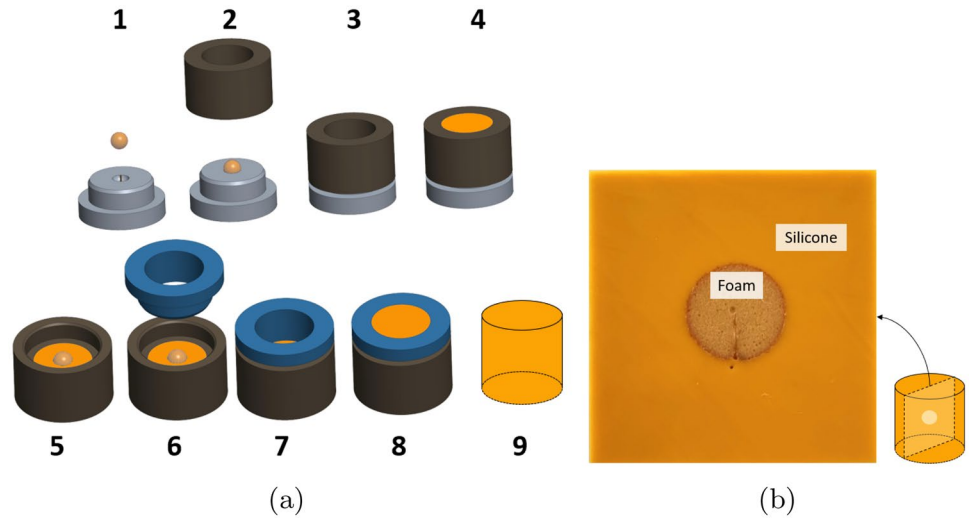
The resulting cylinders typically have a diameter of $29.8 \pm 0.02 \text{ mm}$. Figure 3(b) shows a sample obtained this way. No voids were observed at the foam/silicone interface after testing. The bond between the two materials is therefore assumed to be maintained during the test. Consequently, there is no fluid exchange between the interior and exterior of the foam, neither during molding, nor during the test.

Apparatus and Test Protocol

Once the silicone is molded around the foam sample, the [foam+silicone] sample is put in a confined compression chamber made of steel, with a cavity diameter of 30 mm. Therefore, there is initially a small gap, of around 0.2 mm, between the diameter of the silicone cylinder and the internal diameter of the chamber. To reduce the friction between the specimen and the chamber, a lubricant (a synthetic oil) is applied on the specimen sides. The whole setup can then be used on a standard compression machine (Fig. 4). The machine used is a servo hydraulic testing machine with a load capacity of 25 kN.

For the tests presented in this paper (a different protocol could be applied), four cycles from -10N to -20kN are performed, with a 1 min pause at -10N between the third and the fourth cycle. This test is used to evaluate the cyclic accommodation and viscoelastic recovery. The tests are displacement-driven. A constant displacement rate of approximately 0.3 mm/s is applied during loading and unloading. The displacement rate at the end of loading and at the beginning of unloading is slightly slower, due to machine control. The tests presented are performed at room temperature. Similar tests are also carried out on silicone cylinders alone (without foam inside) to obtain the data required for post-processing the tests with [foam+silicone] sample, as discussed below. The available data from the test are the piston displacement and the load measured by the machine load cell.

Fig. 3 Molding process steps (a) and sample cut in two, in a radius-height plane passing through the cylinder axis for visualization (b)



FEA Model

Some steps of the post-processing are justified by FEA simulations, carried out with Abaqus, using an implicit procedure. The system is modelled in 2D using the axisymmetric hypothesis. The chamber is modelled by an analytical rigid surface (Fig. 5). Linear hybrid elements are used to mesh both foam and silicone parts. The displacement is applied to the piston, modelled by an analytical rigid surface. Adhesion between foam sample and silicone is assumed to be perfect. A gap of 0.1 mm is considered between the silicone cylinder outer surface and the chamber, in line with the experiments. Contact

using isotropic Coulomb friction is defined between the silicone cylinder upper and bottom surfaces and the piston and the chamber. A coefficient of friction of 0.3 is defined so that the results of the FEA are consistent with the experimental data (see section “[Detection of the Effective Start of the Test](#)”). As discussed in the following, the value of this coefficient, as long as it is non-zero, is of little importance given the post-processing established. Between the cylinder lateral surface and the chamber, a frictionless contact is introduced as a first approach. Indeed, this surface was lubricated before testing. The influence of friction will be discussed in section “[Validation of the Test and the Post-processing](#)”.

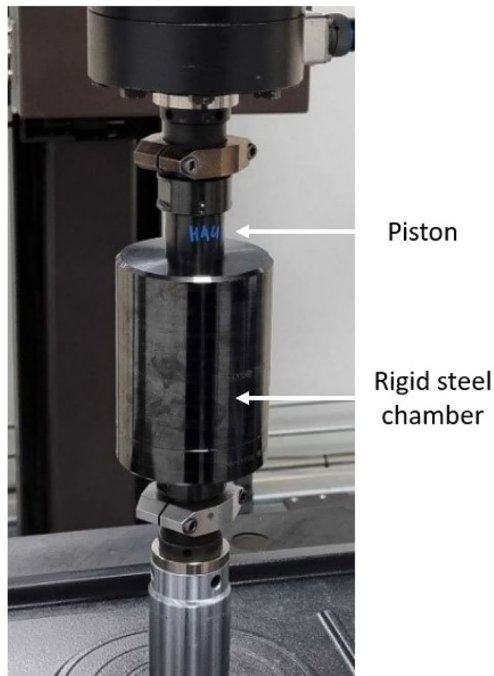


Fig. 4 Confined compression chamber installed on the machine

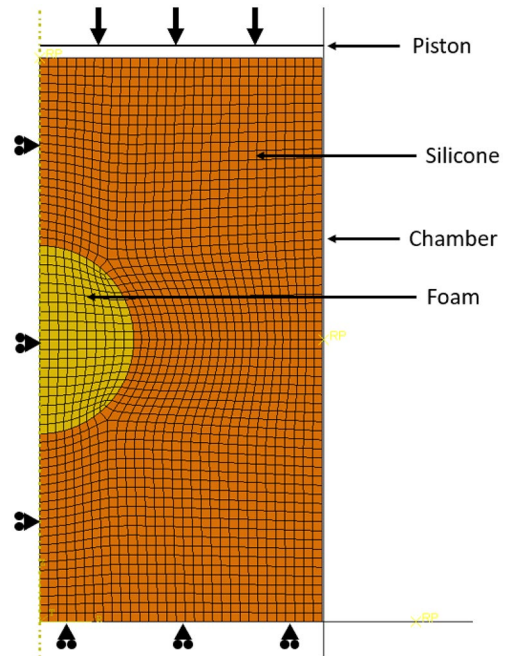


Fig. 5 FEA model (axisymmetric)

The model proposed in [23] is used, via a user subroutine provided by Landauer et al., to describe the compressible hyperelastic behavior of the foam. The model parameters have been identified on an experimental database composed of uniaxial tension, uniaxial compression, simple shear and confined compression tests as presented in [24], performed on the same MCU material as the one used in this paper. The data used for identification, the constitutive equations and model parameters can be found in the Appendix. A polynomial hyperelastic model of second order is used to describe the silicone behavior [25]. The built-in model by Abaqus has been identified on the basis of results from a uniaxial compression test and a confined compression test on the silicone sample (see Appendix).

Post-processing Procedure

Correction of the Machine Stiffness

The setup has a certain compliance. The displacement actually applied to the sample is therefore not equal to the displacement measured. To correct it, a test with no specimen inside the chamber (piston in contact with the bottom of the chamber) is performed. For a same load, the displacement actually applied to the specimen is then obtained from the difference between the displacement measured on the specimen and the displacement measured with no specimen in the chamber. Figure 6 shows the effect of this correction on the load–displacement curves.

The two main challenges of the post-processing are to infer the volume ratio and the pressure of the foam sample from the load–displacement data obtained on the [foam+silicone] sample.

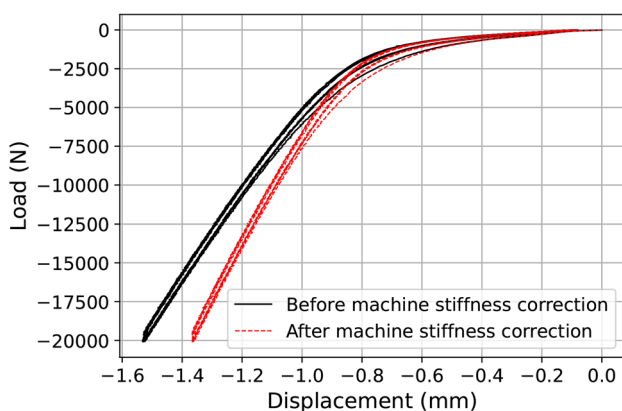


Fig. 6 Load–displacement response of a [silicone+foam] sample before and after taking account of the machine stiffness

Detection of the Effective Start of the Test

Because the silicone cylinder diameter is slightly smaller than the inner diameter of the chamber (the difference is about 0.2 mm), the specimen is in fact mostly under uniaxial compression at the very beginning of the test.

Experimentally, the detection of the onset of the effective expected hydrostatic compression can only be based on the overall load–displacement response (Fig. 7(a)). Figure 7(b) shows the derivative of the load–displacement signals calculated by FEA and measured during one test (the experimental data have been smoothed using a Savitzky-Golay filter [26]). FEA and experimental results show a significant increase in the derivative of the load–displacement signal beyond a given displacement (approximately -0.35 mm in Fig. 7(b)). FEA results show that the increase in the derivative corresponds to the cylinder coming into contact with the chamber. In Fig. 7, the square marks correspond to the moment when the contact just begins and the triangle marks to the moment when the specimen is fully in contact with the chamber. Indeed, due to friction on its upper and lower surfaces, the cylinder does not deform completely homogeneously before it comes into contact with the chamber wall: it takes the shape of a barrel. As a result, the entire lateral surface of the cylinder does not come into contact with the chamber at the same time. The moment when full contact occurs is associated with a maximum on the derivative of the load–displacement data. In FEA, the value of the friction coefficients (between the top and bottom faces of the cylinder and the piston and the bottom of the chamber, respectively) has an effect on the slope between the first contact and full contact points. However, this does not affect the method for detecting the effective start of the test (as described below) and the rest of the post-processing. The slight decrease of the load derivative after full contact is due to a material effect: as shown in Fig. 17, foam rigidity decreases at the start of deformation (before a densification phase).

According to FEA, the hydrostatic stress-volume ratio response of the foam obtained by processing the force and displacement data is very close to the response expected in purely hydrostatic compression (according to the predictions of the behaviour law) when the actual start of the test is taken at a point intermediate between first contact and full contact. The influence of the effective starting point on the results will be discussed in section “Validation of the Test and the Post-processing”. Based on these results, it is decided to consider that the hydrostatic compression test starts when the derivative of the force is the average of the maximum and minimum values of the derivative on both sides of this transition. This point at mid-height (circular points in Fig. 7) is determined for each loading cycle.

Stress and Volume Ratio of the [foam+silicone] Sample

Once the point corresponding to the effective start of hydrostatic compression has been defined, the mean hydrostatic Cauchy stress in the [foam+silicone] sample and its volume ratio are set to 0 and 1, respectively, and the specimen geometry is updated (the validity of this post-processing is discussed in section “[Validation of the Test and the Post-processing](#)”). As confirmed by FEA, the mean hydrostatic stress in the [foam+silicone] sample σ_{F+S} is almost equal to the mean hydrostatic stress in the silicone σ_S during the entire test. Since silicone is nearly incompressible, σ_S which is approximately equal to the axial stress which can be determined as estimated when there is no friction between the cylinder’s lateral surface and the chamber:

$$\sigma_{F+S} \approx \sigma_S \approx \frac{F - F_c}{S} \quad (1)$$

where F is the global force, F_c is the global force corresponding to the effective start of the expected hydrostatic compression (algebraic value) and S is the surface area of the cross section of the chamber (perpendicular to its axis). The volume ratio J_{F+S} of the [foam+silicone] sample is calculated as follows:

$$J_{F+S} = 1 + \frac{D - D_c}{H_0 + D_c} \quad (2)$$

where D is the global displacement, D_c is the displacement at the effective start of the test (algebraic value) and H_0 is the initial height of the sample. Figure 8 shows an example of results obtained.

Volume Ratio of the Foam Sample

To determine the mean foam volume ratio J_F , the following equation is used:

$$J_F = \frac{1}{V_{0,F}} \times (J_{F+S} \times V_{0,F+S} - J_S(\sigma_S) \times (V_{0,F+S} - V_{0,F})) \quad (3)$$

$V_{0,F}$ and $V_{0,F+S}$ are the initial mean volumes of the foam sample and of the [foam+silicone] sample, respectively. J_{F+S} is the mean volume ratio of the [foam+silicone] sample. J_S is the mean volume ratio of silicone, depending on the mean hydrostatic Cauchy stress σ_S to which it is subjected. The relationship between J_S and σ_S is obtained from a confined compression test performed with the same device on a silicone cylinder without foam inside. In this case, the confined compression test is assumed to start at the peak in the evolution of the derivative of the load–displacement curve, i.e., when the specimen is fully in contact with the chamber wall. In this case, the transition is very abrupt and first and full contacts are very close together. σ_S and J_S are calculated using equations similar to equations (1) and (2), but applied to a silicone specimen.

It is assumed that the foam sample has no residual deformation and is still in contact with the silicone at the start of each cycle. Furthermore, to ensure that the results are not biased by potential side effects from the cycling of the silicone, such as the Mullins effect, each cycle applied to the [foam+silicone] specimen is associated with the same cycle applied to the silicone specimen alone.

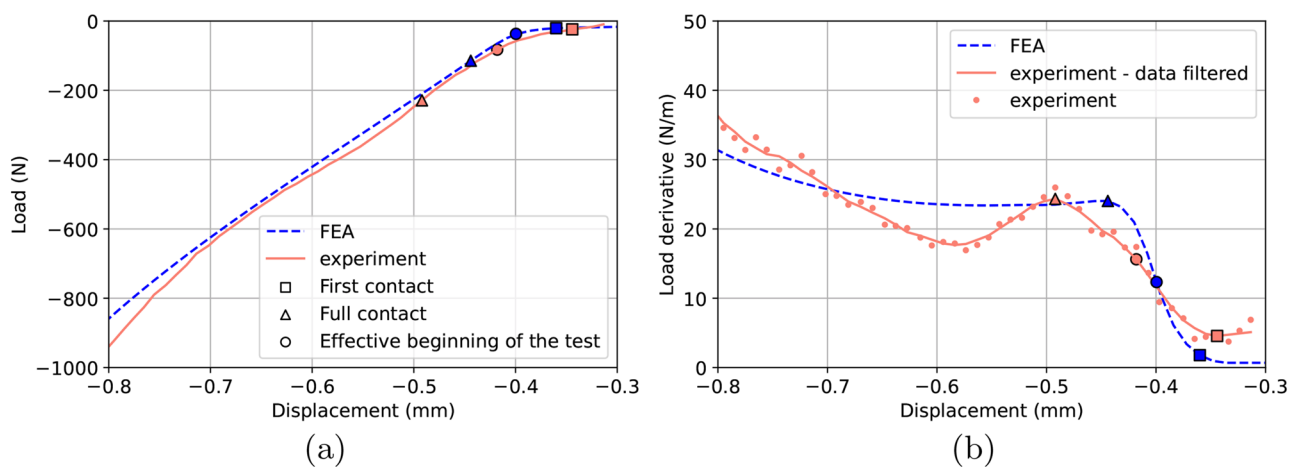


Fig. 7 Load–displacement (a) and derivative of the load–displacement (b) signals for the [foam+silicone] sample calculated by FEA and experimentally measured at the beginning of the loading; the circular points represent the start of the expected hydrostatic compression test according to FEA and to the detection method used to process the experiments, respectively; the square and triangle correspond to the first and full contact between the specimen and the walls of the chamber, respectively

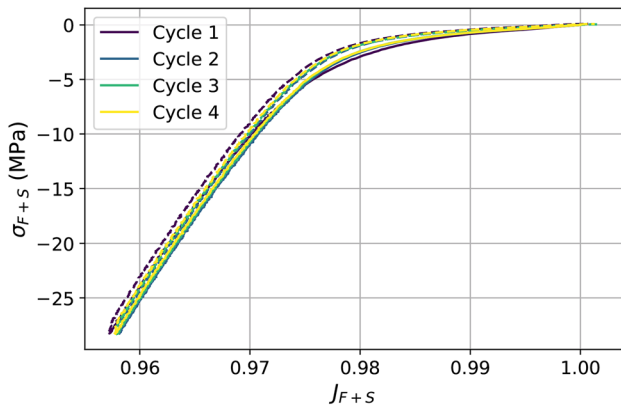


Fig. 8 Mean Cauchy hydrostatic stress in the [foam+silicone] sample as a function of its volume ratio for the four cycles performed on a [foam+silicone] sample (load step in solid lines and unload step in dashed lines)

Hydrostatic Stress in the Foam Sample

The mean hydrostatic Cauchy stress in the foam sample σ_F is not equal to the mean hydrostatic Cauchy stress in the silicone σ_S . The objective here is thus to find a localization relationship to connect σ_F and σ_S , independent from the foam mechanical behavior.

The hydrostatic stress difference between the foam and the silicone $\Delta\sigma = \sigma_F - \sigma_S$ depends on the ratio between the compressibilities of the foam and the silicone. The bulk modulus of the silicone used is approximately equal to 1430 MPa throughout the test. The bulk modulus of the foam depends in particular on the material density and varies during the test. The initial compressibility modulus of the foams studied here is of the order of a few MPa. Figure 9(a) gathers the simulation results obtained using four different initial bulk moduli B_i for the foam (the other parameter values remain unchanged), between 0.2 and 200 MPa.

Figure 9(b) shows the evolution of $\Delta\sigma$ as a function of J_F calculated by FEA. The results show that $\Delta\sigma$ is the same for the three lowest bulk moduli used, but is slightly different for the highest. This illustrates the fact that $\Delta\sigma$ does not depend on the behavior of the foam sample as long as its bulk modulus is much lower than the bulk modulus of silicone (by a factor higher than 100 typically). This is consistent with the results of the analytical study conducted in [27] for a spherical compressible liquid inclusion embedded in a linear elastic matrix.

Therefore, the master curve of $\Delta\sigma(J_F)$ in Fig. 9(b) is considered valid when the foam compressibility is 100 times lower than the silicone one. As the silicone used has a bulk modulus of 1430 MPa, the pressure localization relationship $\Delta\sigma(J_F)$ is valid until the foam reaches a instantaneous bulk modulus of about 14 MPa. This means that the localization

relationship is no longer appropriate during the densification phase (when the majority of cells in the foam are closed), where the foam becomes nearly incompressible. Nevertheless, during this phase, the volume ratio of the foam does not vary much so that the error on pressure does not prevent the accurate identification of the densification phase.

As previously mentioned, the behavior law identified for silicone on confined compression also contains the effect of friction between the specimen and the chamber wall. This approach allows to access the hydrostatic Cauchy stress in the foam from the measured force (which includes the effect of friction), without having to explicitly quantify the effect of friction. So, finally, the average hydrostatic Cauchy stress in the foam sample σ_F is estimated from σ_{F+S} calculated using equation (1) and from $\Delta\sigma(J_F)$, with J_F determined using equation (3):

$$\sigma_F \approx \Delta\sigma(J_F) + \sigma_{F+S} \quad (4)$$

Validation of the Test and the Post-processing

Post-processing Procedure

Figure 10 shows the mean hydrostatic Cauchy stress-volume ratio response of the foam obtained using the established post-processing procedure (mid-height contact; see Fig. 7(b)), applied to FEA results. The results are compared to the exact response predicted by the constitutive model (see Appendix) for perfect hydrostatic compression and to the response obtained from the mean values of the hydrostatic stress and the volume ratio calculated by FEA in the foam sample. The two other curves correspond to the responses obtained by considering the points of first contact and full contact (as defined in section “Detection of the Effective Start of the Test”) to determine the effective start of the test. On the one hand, the comparison shows that the hydrostatic stress-volume ratio response calculated by FEA on average in the sample is very close to that expected for perfectly hydrostatic compression. On the other hand, the comparison shows that the result is sensitive to the point considered for the actual start of the test. At last, the figure proves that the post-processing procedure established provides a good estimation of the foam response to hydrostatic compression, from the global load and displacement measured. In the example shown in Fig. 10, the initial slope (calculated by linear regression in the volume ratio range 0.9-1) is underestimated by about 14% and the volume ratio at

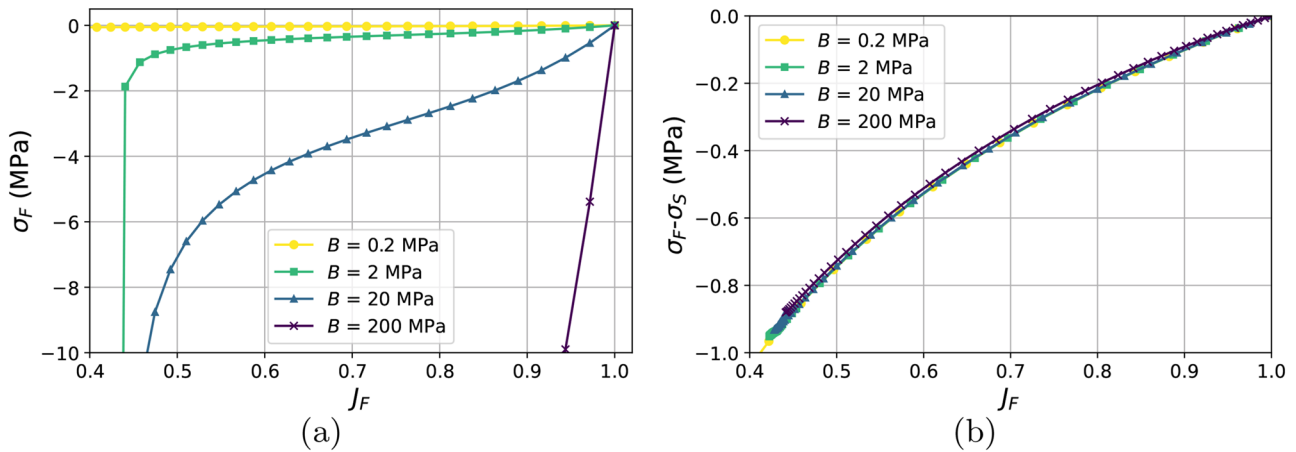


Fig. 9 FEA study of the influence of the initial bulk modulus of the foam on its response to hydrostatic compression (a) and on the difference between the hydrostatic Cauchy stresses in the foam and in the silicone (b)

densification (defined as the volume ratio for an arbitrary hydrostatic stress value of -10 MPa) is overestimated by about 1.3%. The deviation at the beginning of load is due to contact detection and load reset to 0.

Strain and Stress States

Figure 11 shows the fields of hydrostatic pressure and volume ratio in the [foam+silicone] sample calculated by FEA (as described in section “FEA Model”). According to the simulation, the volume ratio and the hydrostatic Cauchy stress fields are relatively homogeneous in the foam sample: on the entire load range, they vary by a maximum of 0.7% and 2% in the foam sample, respectively. In addition, the sample keeps a relatively spherical shape even at high strains levels. The ratio

between the minor and major axis of the ellipse is between 1 and 0.9 before densification (see Fig. 11), and decreases to about 0.85 after densification. The foam sample does not remain completely spherical, mainly because the [foam+silicone] sample is subjected to quasi-uniaxial compression at the very beginning of the test, before the gap between the cylinder surface and the compression chamber is completely closed.

To better characterize the stress state in the foam sample, a stress triaxiality angle θ_σ is defined [28]:

$$\theta_\sigma = \arctan \frac{\frac{1}{3} \text{Tr}(\underline{\underline{\sigma}})}{\sqrt{\frac{3}{2} \text{dev}(\underline{\underline{\sigma}}) : \text{dev}(\underline{\underline{\sigma}})}}$$

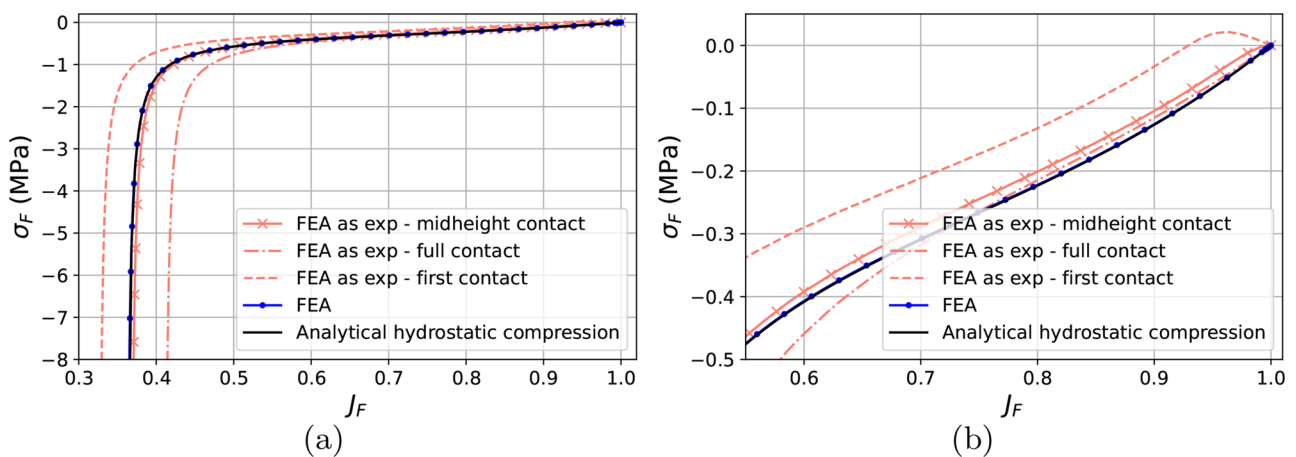
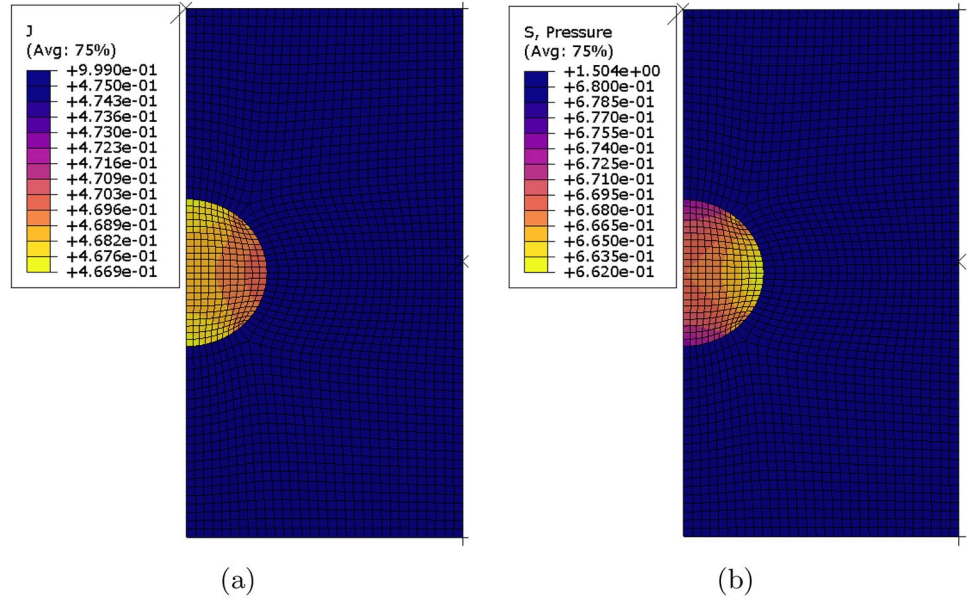


Fig. 10 Hydrostatic stress-volume ratio response (full range (a) and zoom (b)) obtained for the foam by applying to FEA results the protocol presented above to derive these quantities from force and displacement data, by taking the effective start of the test (as defined in Fig. 7(b)) at mid-height contact, at full contact or at first contact, compared to the response obtained by FEA by calculating the mean values of the hydrostatic stress and volume ratio of the foam sample, and to the analytical response for perfect hydrostatic compression

Fig. 11 Volume ratio (a) and hydrostatic pressure (in MPa) (b) calculated by FEA of the hydrostatic compression test



where $\underline{\underline{\sigma}}$ is the Cauchy stress tensor, $\text{Tr}(\underline{\underline{\sigma}})$ is the trace of $\underline{\underline{\sigma}}$, $\underline{\underline{\text{dev}}}(\underline{\underline{\sigma}})$ is the deviatoric part of $\underline{\underline{\sigma}}$ and $:$ is the inner product. In the same way, a strain triaxiality angle θ_ϵ is defined as follows:

$$\theta_\epsilon = \arctan \frac{\frac{1}{3} \text{Tr}(\underline{\underline{\epsilon}}_H)}{\sqrt{\frac{2}{3} \underline{\underline{\text{dev}}}(\underline{\underline{\epsilon}}_H) : \underline{\underline{\text{dev}}}(\underline{\underline{\epsilon}}_H)}}$$

where $\underline{\underline{\epsilon}}_H$ is the Hencky strain tensor, calculated from the left stretch tensor $\underline{\underline{V}}$: $\underline{\underline{\epsilon}}_H = \ln \underline{\underline{V}}$. The angle of triaxiality takes some remarkable values at particular stress and strain states:

- In true hydrostatic compression: $\theta_\sigma = -\frac{\pi}{2}$;
- In true volumetric compression: $\theta_\epsilon = -\frac{\pi}{2}$;
- In uniaxial compression: $\theta_\sigma = \arctan -\frac{1}{3} = -0.32$;
- In confined compression: $\theta_\epsilon = \arctan -\frac{1}{3} = -0.32$.

Figure 12 shows the stress and strain triaxiality angles (mean values in the foam sample) calculated by FEA as a function of the mean foam volume ratio. The vertical line corresponds to the effective beginning of the test as defined in section “[Detection of the Effective Start of the Test](#)”. Stress and strain triaxialities change significantly at the beginning of loading. They tend to stabilize below a volume ratio of about 0.9. θ_σ starts from a value close to that expected for uniaxial compression (-0.32) at the very beginning of the test and becomes close to the one expected for hydrostatic compression ($-\pi/2$) when the volume ratio is lower than

0.9. θ_ϵ remains different from that expected in volumetric compression ($-\pi/2$). It is nevertheless significantly higher (in absolute value) than the one expected in confined compression (-0.32). The foam sample is not subjected to a perfect volumetric/hydrostatic compression because the cylinder is not immediately in confined compression due to the initial gap between its lateral surface and the compression chamber wall. The foam slightly loses its sphericity at the start of the test. According to these results, the foam sample is subjected to a loading closer to hydrostatic compression than to volumetric compression. The stress state is close to that of hydrostatic compression for volume ratios below 0.9 (for a gap of 0.2 mm between the cylinder and the chamber), up to the densification phase (volume ratio of about 0.35 in the example shown in Fig. 12).

Influence of Bulk Modulus Ratio

One question raised in section “[Hydrostatic Stress in the Foam Sample](#)” is the influence of the relative ratio of the compressibility of the silicone and the foam. In the case of the example in Fig. 10, the ratio between the bulk modulus of silicone and that of foam becomes less than 100 for a foam volume ratio lower than about 0.42. The pressure localization relationship used to estimate the hydrostatic stress in the foam sample from the mean stress in the [foam+silicone] sample becomes less accurate for lower volume ratios. Nevertheless, the response obtained remains acceptable, since the volume ratio varies little with respect to hydrostatic stress. However, the final slope, when densification occurs, is not representative of the foam’s bulk modulus because the foam becomes almost incompressible (the cells are closed), with a bulk modulus significantly higher than that of silicone.

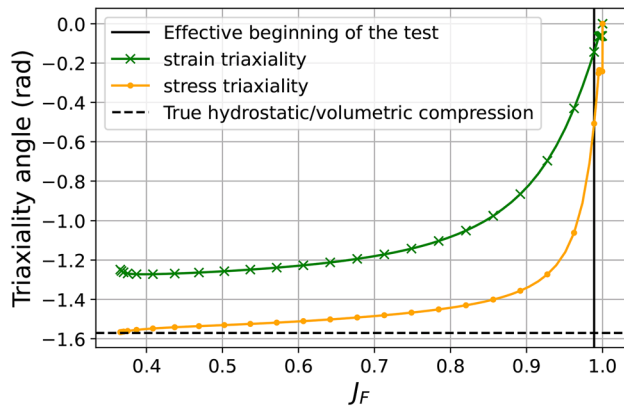


Fig. 12 Average stress and strain triaxiality angles in the foam sample, calculated by FEA

Influence of Friction

As mentioned in section “Procedures”, the FEA simulations presented above were carried out with no friction between the cylinder’s lateral surface and the chamber. Prior to the tests presented in the following section, the cylinder’s lateral surface was lubricated to limit friction. The coefficient of friction is therefore probably low but not zero. Experimentally, it can be difficult to accurately estimate the coefficient of friction. Simulations have shown that friction has relatively little effect on strain and stress states: as the friction coefficient increases, the absolute value of the strain triaxiality angle decreases slightly (by a maximum of 0.15), while the stress triaxiality angle remains almost unchanged. Figure 13 shows a sensitivity study of the value of the coefficient of friction between the cylinder’s lateral surface and the chamber, based on FEA.

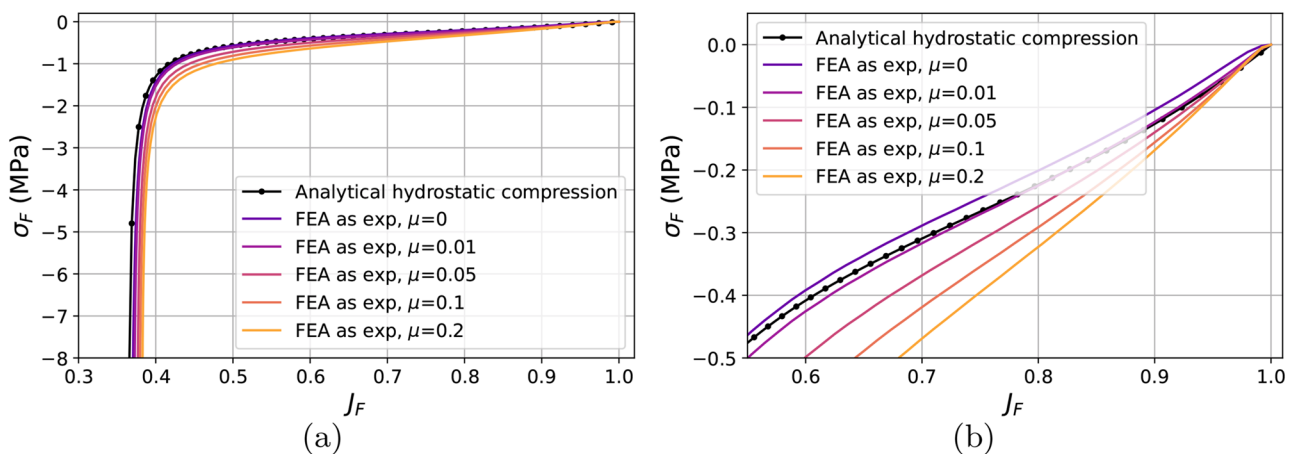


Fig. 13 Hydrostatic stress-volume ratio response (full range (a) and zoom (b)) of the foam as determined by applying the post-processing protocol presented above to FEA results obtained for several coefficients of friction μ between the cylinder’s lateral surface and the chamber, compared to the analytical response for perfect hydrostatic compression

The results show that friction has a non-negligible but limited effect on hydrostatic stress-volume ratio response determined by applying the proposed post-processing protocol proposed to FEA results. Tests with and without lubrication have confirmed this trend. In Fig. 13, compared to the analytical case for a perfect hydrostatic compression, a friction coefficient of 0.05 leads to an overestimation of the initial slope (in the 0.9-1 volume ratio range) by about 14% and to an overestimation of the volume ratio at densification (for a hydrostatic stress value of -10 MPa) by about 3.3%.

Results and Discussion

Results of the Tests

Figure 14 shows examples of mean hydrostatic Cauchy stress vs. volume ratio curves obtained for the four loading cycles applied to one specimen, with a foam sample of density 354 kg.m^{-3} . The trends are in line with expectations for this type of material [7, 29]. The densification phase is clearly visible from a volume ratio below approximately 0.35. A stress softening is observed between the first and the second cycles. The response then stabilizes. This cyclic stress softening is expected in elastomers [30]. Note that the test cannot give information on the potential residual deformation of the foam after a cycle (see section “Volume Ratio of the Foam Sample”).

Figure 15 shows the results of 15 tests performed on foam balls of different densities from 350 to 560 kg.m^{-3} . Only the loading of the first cycle is shown. The curves are ranked consistently: the denser the foam, the stiffer its response and the lower the volume ratio at densification.

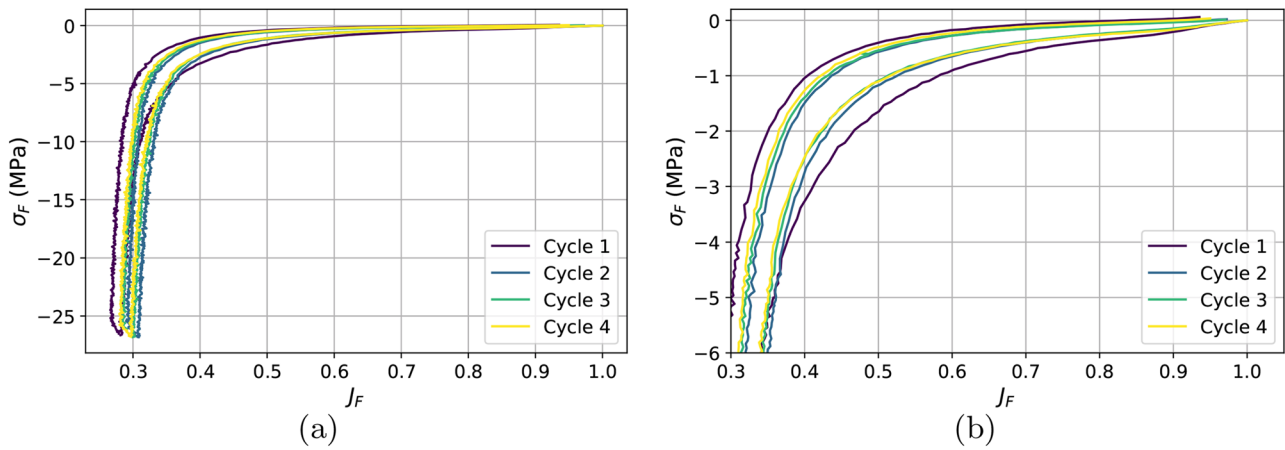


Fig. 14 Mean hydrostatic compression curve for a foam density of 354 kg.m^{-3} ; full range (a) and zoom (b)

These results show that the proposed test allows to reach the target volume ratios (0.3 typically) and hydrostatic stress levels (-25 MPa typically). Furthermore, with the post-processing protocol implemented, the test is sensitive enough to observe relatively small material effects, such as cyclic softening or the influence of material density.

Discussion on the Results Obtained: Trends and Scattering

Two indicators are used to discuss the results: the initial bulk modulus and the volume ratio at densification. A linear dependence of these quantities on the density can be expected in the range investigated [7, 31]. The initial bulk modulus is calculated by linear regression in the volume ratio range 0.9-1. The volume ratio at densification is determined for an arbitrary hydrostatic stress value of -10 MPa. Figure 16 shows the initial bulk modulus at the first loading and the volume ratio at densification

determined for the 15 tests presented above. The general trend as a function of density is consistent with expectations. The scattering is about the same for both quantities (coefficient of determination R^2 of 0.77–0.78). In Fig. 16(b), the dotted red lines correspond to expected trends for the minimum and maximum density values for bulk polyurethane reported in the literature [32, 33]. The volume ratio at densification is equal to the ratio of the density of the foam to the density value of the bulk material (not foamed). Most of the points (80%) obtained are in this range. This confirms that the results obtained are relevant.

Several factors may explain the scattering observed. A first potential source of scattering is the friction between the cylinder’s lateral surface and the chamber that may vary one test to another, despite the precautions taken. A second factor is the detection of the actual start of the hydrostatic compression test, linked to contact between the specimen and the chamber. Because the measured displacement is very small and because of experimental noise, it is sometimes

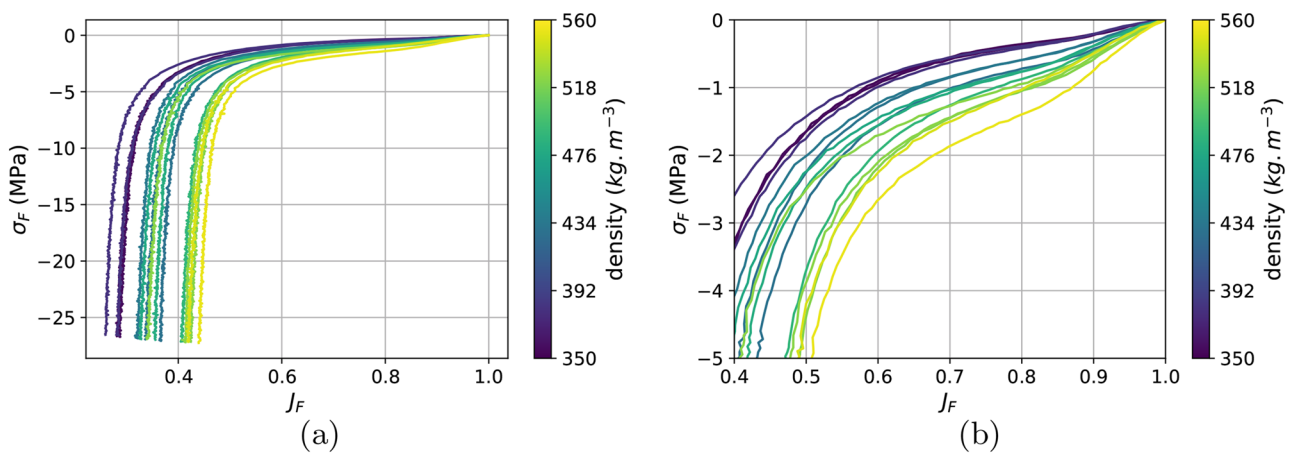


Fig. 15 Mean hydrostatic compression curves for foams of various densities; full range (a) and zoom (b)

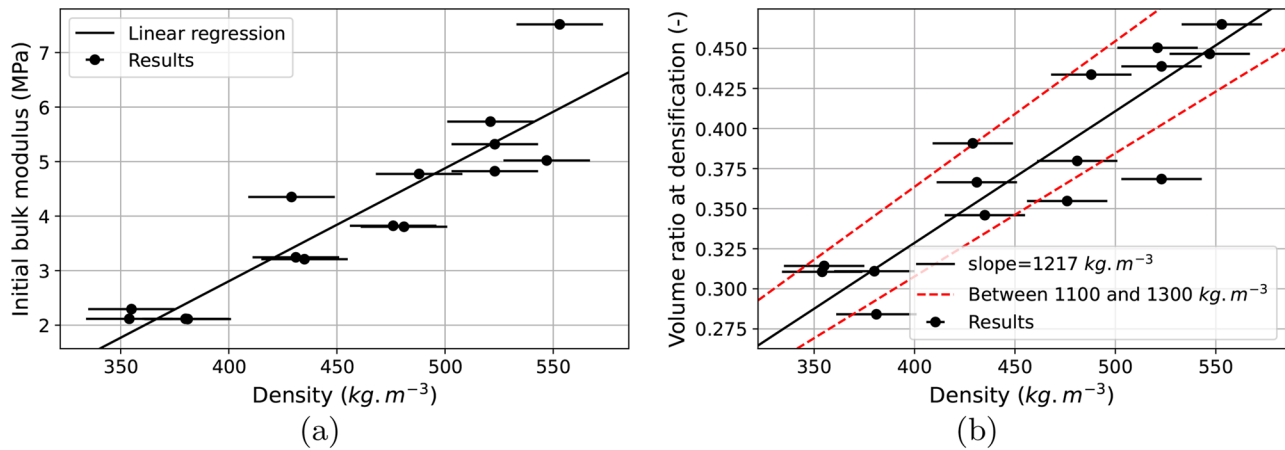


Fig. 16 Initial bulk modulus (a) and volume ratio at densification (b) obtained from the test results as a function of the density of the foam sample (the dotted lines on the right figure correspond to the volume ratios at densification expected from the material densities considering densities of 1100 and 1300 kg.m^{-3} for the bulk material); horizontal lines correspond to the uncertainty in the value of the sample density

difficult to detect the contact accurately. A third factor is the measurement error on the foam sample diameter: as the test is performed on a small foam specimen, any small measurement errors lead to different results. The scattering could be reduced by increasing the specimen and device dimensions.

Conclusions

This paper presents an original test to characterize the response of polymeric foams under hydrostatic compression, called SFIR. A cylinder of dense, nearly-incompressible elastomer is molded around a sample of the polymeric foam to be tested, machined in the form of a sphere. The set is then subjected to a classic confined compression test in a rigid chamber. Finite element simulations show that the foam sample is subjected to nearly hydrostatic compression, leading to large volume variations. A post-processing protocol is established, on the basis of FEA, to determine the volume ratio and the hydrostatic stress of the foam from the global load and displacement data measured during the test. The protocol requires carrying out a test under the same conditions on the nearly-incompressible elastomer cylinder alone (without the foam sample). A relationship is established to calculate the hydrostatic stress in the foam from the overall force. This relationship is valid whatever the behavior of the foam as long as its bulk modulus is very small compared to that of the bulk elastomer used for the cylinder surrounding the foam sample (bulk modulus ratio of typically

100) and can be used for any foam. The results obtained on fifteen MCU samples with different densities are in line with expectations, with limited scattering.

Contrary to tests where the loading is applied to the foam sample by a fluid or a gas, the test proposed does not cause security issues linked, for example, to sealing. It could be easily implemented in academic or industrial laboratories with limited equipment. High pressures can be reached easily as long as the chamber in which the specimen is placed does not deform significantly. Large volume variation can be applied to the foam sample without difficulty. This test can also be used to characterize the response to nearly hydrostatic compression of any kinds of highly compressible polymeric foams, with open or closed cells, under conditions where there is no exchange of fluid between the inside of the foam and the outside).

Appendix: Constitutive Models used for the Foam and the Silicone

The model proposed in [23] is used to describe the compressible hyperelastic behavior of the foam. It is based on the invariants K_1 , K_2 and K_3 derived from the Hencky strain tensor $\underline{\underline{\varepsilon}}_H$, calculated from the left stretch tensor $\underline{\underline{V}}$: $\underline{\underline{\varepsilon}}_H = \ln \underline{\underline{V}}$ [34]. The Hencky strain tensor can indeed be decomposed in a volume and deviatoric part: $\underline{\underline{\varepsilon}}_H = \frac{1}{3}K_1\underline{\underline{I}} + K_2\underline{\underline{N}}$, where $K_1 = \text{Tr} \left(\underline{\underline{\varepsilon}}_H \right)$ with

$\text{Tr} \left(\underline{\underline{\varepsilon}}_H \right)$ the trace of $\underline{\underline{\varepsilon}}_H$, $K_2 = \sqrt{\underline{\underline{\text{dev}}}(\underline{\underline{\varepsilon}}_H) : \underline{\underline{\text{dev}}}(\underline{\underline{\varepsilon}}_H)}$ with $\underline{\underline{\text{dev}}}(\underline{\underline{\varepsilon}}_H)$ the deviatoric part of $\underline{\underline{\varepsilon}}_H$ and $:$ the inner product, $\underline{\underline{I}}$ is the second-order identity tensor and $\underline{\underline{N}}$ is a deviatoric unit-magnitude tensor. K_3 is defined as $K_3 = 3\sqrt{6} \det(\underline{\underline{N}})$, where $\det(\underline{\underline{N}})$ is the determinant of $\underline{\underline{N}}$. The strain energy potential $W_F(K_1, K_2, K_3)$ writes:

$$W_F(K_1, K_2, K_3) = G_0 [X(K_1)K_2^2 + L(K_2, K_3)] + Bf(K_1) \quad (\text{A1})$$

with:

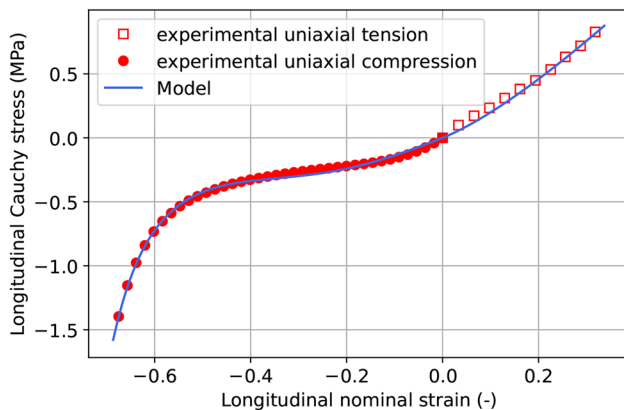
$$X(K_1) = \frac{1}{2}(X'_1 + X'_2)K_1 + \frac{\Delta_K}{2}(X'_1 - X'_2) \ln \left(\frac{\cosh((K_1 - K_1^0)/\Delta_K)}{\cosh(K_1^0/\Delta_K)} \right) + 1 \quad (\text{A2})$$

$$L(K_2, K_3) = C_0 K_2^p + C_1(1 + K_3)K_2^q \quad (\text{A3})$$

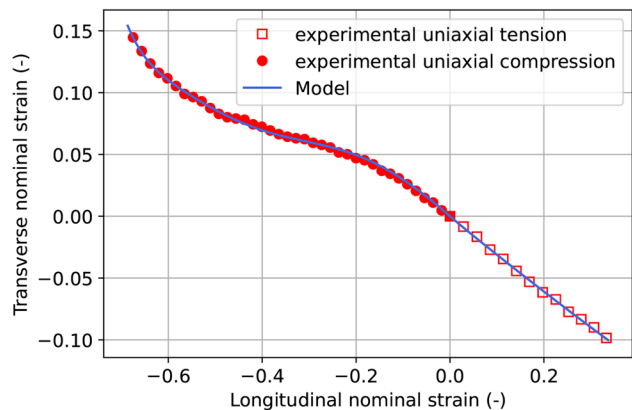
$$f(K_1) = \frac{J_F(K_1)^{C_2} - C_2 \ln J_F(K_1) - 1}{C_2^2} + \frac{C_3}{r-1} \left[-J_F(K_1)^{1-r} + \frac{(1 - J_{min})^r}{(J_F - J_{min})^{r-1}} + J_{min} \right] \quad (\text{A4})$$

where $J_F = \exp(K_1)$ is the volume ratio. The experimental database used to identify this model is composed of uniaxial compression, uniaxial tension, simple shear and confined compression tests. The experimental results and the response calculated by the model once identified are shown in Fig. 17. The model parameter values identified are gathered in Table 1.

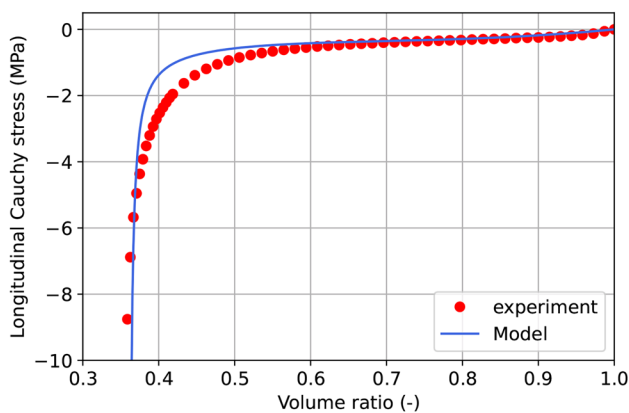
The model used for the silicone is a polynomial hyper-elastic model for slightly compressible materials, where the potential strain energy W_S writes:



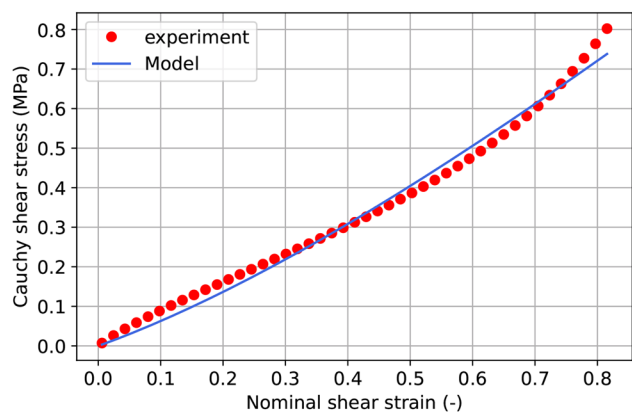
(a) Loading direction.



(b) Transverse direction.



(c)



(d)

Fig. 17 Experimental response and response calculated by the model for the foam in uniaxial compression and tension (a, b) (longitudinal stress-longitudinal strain response and longitudinal strain-transverse strain response, respectively), confined compression (c) and simple shear (d)

Table 1 Parameter values of the model identified to describe the behavior of the MCU foam

G_0 (MPa)	B (MPa)	J_{min} (-)	C_1 (-)	K_1^0 (-)	Δ_K (-)	X_1' (-)
0.666	2.02	0.430	1.00	-0.109	0.392	4.15
X_2' (-)	C_0 (-)	p (-)	q (-)	r (-)	C_2 (-)	C_3 (-)
0	0.106	5.02	2.74	0.664	9.09	0.0545

$$W_S = \sum_{i+j=1}^2 C_{ij}(\bar{I}_1 - 3)^i(\bar{I}_2 - 3)^j + \sum_{k=1}^2 \frac{1}{D_k}(J_S - 1)^{2k} \quad (A5)$$

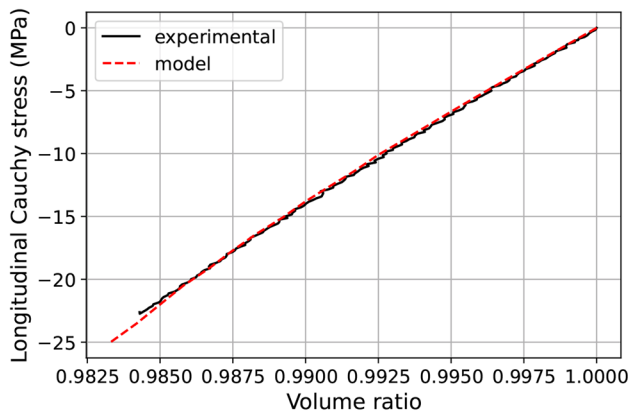
where $\bar{I}_1 = J_S^{-2/3}I_1$ and $\bar{I}_2 = J_S^{-4/3}I_2$ with I_1 and I_2 the two main invariants of the left Cauchy-Green deformation tensor and J_S the volume ratio. The model parameters have been

identified using results from confined compression and uniaxial compression tests. The parameters identified are given Table 2.

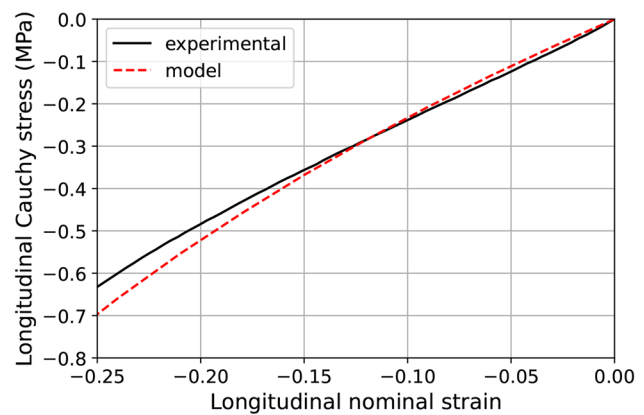
Figure 18 presents the experimental curves and the responses calculated with the model.

Table 2 Parameter values of the model identified to describe the behavior of silicone

C_{10} (MPa)	C_{01} (MPa)	C_{11} (MPa)	C_{02} (MPa)	C_{20} (MPa)	D_1 (MPa ⁻¹)	D_2 (MPa ⁻¹)
0.0622	0.292	0	0	0	1.52·10 ⁻³	6.01·10 ⁻⁶



(a)



(b)

Fig. 18 Experimental and model responses for silicone in confined compression (a) and uniaxial compression (b)

Funding This work was supported by the French ANRT agency (CIFRE n°2021/1340).

Declarations

Conflict of interest The authors have no Conflict of interest to declare that are relevant to the content of this article.

References

- Bridgman PW (1946) Recent work in the field of high pressures. *Rev Mod Phys* 18(1):1–93. <https://doi.org/10.1103/RevModPhys.18.1>. Publisher: American Physical Society
- Birch F, Dow RB (1936) Compressibility of rocks and glasses at high temperatures and pressures: seismological application. *GSA Bull* 47(8):1235–1255. <https://doi.org/10.1130/GSAB-47-1235>
- Bailey AC, Johnson CE, Schafer RL (1986) A model for agricultural soil compaction. *J Agric Eng Res* 33(4):257–262. [https://doi.org/10.1016/S0021-8634\(86\)80040-3](https://doi.org/10.1016/S0021-8634(86)80040-3)
- Singh SK, Jordaan IJ (1986) Triaxial tests on crushed ice. *Cold Reg Sci Technol* 24(2):153–165. [https://doi.org/10.1016/0165-232X\(95\)00017-6](https://doi.org/10.1016/0165-232X(95)00017-6)
- Ruan D, Lu G, Ong LS, Wang B (2007) Triaxial compression of aluminium foams. *Compos Sci Technol* 67(6):1218–1234. <https://doi.org/10.1016/j.compscitech.2006.05.005>
- Adams LH, Gibson RE (1930) The compressibility of rubber. *Rubber Chem Technol* 3(4):555–562. <https://doi.org/10.5254/1.3535518>
- Viot P (2009) Hydrostatic compression on polypropylene foam. *Int J Impact Eng* 36(7):975–989. <https://doi.org/10.1016/j.ijimpeng.2008.11.010>
- Masso Moreu Y, Mills NJ (2004) Rapid hydrostatic compression of low-density polymeric foams. *Polym Testing* 23(3):313–322. <https://doi.org/10.1016/j.polymertesting.2003.07.002>
- Ozturk UE, Anlas G (2011) Hydrostatic compression of anisotropic low density polymeric foams under multiple loadings and unloadings. *Polym Testing* 30(7):737–742. <https://doi.org/10.1016/j.polymertesting.2011.06.002>
- Wang YC, Ko CC, Huang YH (2013) Viscoelastic properties of foam under hydrostatic pressure and uniaxial compression. *Procedia Engineering* 67:397–403. <https://doi.org/10.1016/j.proeng.2013.12.039>
- Kim Y, Kang S (2003) Development of experimental method to characterize pressure-dependent yield criteria for polymeric foams. *Polym Testing* 22(2):197–202. [https://doi.org/10.1016/S0142-9418\(02\)00080-6](https://doi.org/10.1016/S0142-9418(02)00080-6)
- Kumar D, Ruan D, Khaderi SN (2023) Triaxial characterization of foams at high strain rate using split-Hopkinson pressure bar. *Exp Mech*. <https://doi.org/10.1007/s11340-023-00978-3>
- Koprowski-Theiß N, Johlitz M, Diebels S (2012) Pressure dependent properties of a compressible polymer. *Exp Mech* 52(3):257–264. <https://doi.org/10.1007/s11340-011-9489-9>
- Moore B, Jaglinski T, Stone D, Lakes R (2007) On the bulk modulus of open cell foams. *Cell Polym* 26. <https://doi.org/10.1177/026248930702600101>
- Cui J, Hao H, Shi Y, Li X, Du K (2017) Experimental study of concrete damage under high hydrostatic pressure. *Cem Concr Res* 100:140–152. <https://doi.org/10.1016/j.cemconres.2017.06.005>
- Jacobs R (1939) X-ray measurement of compressibility. *Phys Rev* 56:211–212
- Deshpande VS, Fleck NA (2000) Isotropic constitutive models for metallic foams. *J Mech Phys Solids* 48:1253–1283. [https://doi.org/10.1016/S0022-5096\(99\)00082-4](https://doi.org/10.1016/S0022-5096(99)00082-4)
- Bour M, Picart D, Raymond M, Méo S, Chalou F, Le Quilliec G (2022) Dissipative hyperelastic model for highly compressible elastomeric seals. In: *Constitutive models for rubber XII*, pp 26–32. <https://doi.org/10.1201/9781003310266>
- Peng SH, Shimbori T, Naderi A (1994) Measurement of Elastomer's bulk modulus by means of a confined compression test. *Rubber Chem Technol* 67(5):871–879. <https://doi.org/10.5254/1.3538718>
- Le Gall M, Choqueuse D, Le Gac P-Y, Davies P, Perreux D (2014) Novel mechanical characterization method for deep sea buoyancy material under hydrostatic pressure. *Polym Testing* 39:36–44. <https://doi.org/10.1016/j.polymertesting.2014.07.009>
- Zhang J, Kikuchi N, Li V, Yee A, Nusholtz G (1998) Constitutive modeling of polymeric foam material subjected to dynamic crash loading. *Int J Impact Eng* 21:369–386. [https://doi.org/10.1016/S0734-743X\(97\)00087-0](https://doi.org/10.1016/S0734-743X(97)00087-0)
- Le Saux M, Le Bail J-B, Becker J, Caër C, Charrier P, Le Saux V, Maheo L, Marco Y (2023) Statistical characterization of microcellular polyurethane foams microstructure based on 2D and 3D image analysis. *J Cell Plast* 59(5–6):395–417. <https://doi.org/10.1177/0021955X231215773>
- Landauer AK, Li X, Franck C, Henann DL (2019) Experimental characterization and hyperelastic constitutive modeling of open-cell elastomeric foams. *J Mech Phys Solids* 133:103701. <https://doi.org/10.1016/j.jmps.2019.103701>
- Becker J, Le Bail J-B, Le Saux M, Le Saux V, Marco Y, Maheo L, Charrier P, Hervouet W (2022) Modelling of the compressible hyperelastic behavior of polyurethane foams: influence of the identification strategy. In: *Constitutive models for rubber XII*, pp 20–25. <https://doi.org/10.1201/9781003310266>
- Rivlin RS, Saunders D (1951) Large elastic deformations of isotropic materials VII. experiments on the deformation of rubber. *Philosophical Transactions of the Royal Society of London. Series A, Mathematical and Physical Sciences* 243(865):251–288. <https://doi.org/10.1098/rsta.1951.0004>
- Savitzky A, Golay MJ (1964) Smoothing and differentiation of data by simplified least squares procedures. *Anal Chem* 36(8):1627–1639. <https://doi.org/10.1021/ac60214a047>
- Chen X, Li M, Yang M, Liu S, Genin GM, Xu F, Lu TJ (2018) The elastic fields of a compressible liquid inclusion. *Extreme Mechanics Letters* 22:122–130. <https://doi.org/10.1016/j.eml.2018.06.002>
- Donnard A, Guerard S, Maheo L, Viot P, Rio G (2018) Multi-axial experiments with radial loading paths on a polymeric foam. *Polym Testing* 67:441–449. <https://doi.org/10.1016/j.polymertesting.2018.03.003>
- Senol K, Shukla A (2019) Dynamic response of closed cell PVC foams subjected to underwater shock loading. *Int J Impact Eng* 130:214–225. <https://doi.org/10.1016/j.ijimpeng.2019.04.020>
- Mullins L (1969) Softening of rubber by deformation. *Rubber Chem Technol* 42(1):339–362. <https://doi.org/10.5254/1.3539210>
- Senol K, Shukla A (2019) Underwater mechanical behavior of closed cell PVC foams under hydrostatic loading through 3D DIC technique. *Polym Testing* 73:72–81. <https://doi.org/10.1016/j.polymertesting.2018.11.003>

32. Ashby MF, Gibson LJ (1997) Cellular solids: structure and properties. Press Syndicate of the University of Cambridge, Cambridge, UK, pp 175–231
33. Saint-Michel F, Chazeau L, Cavaillé J-Y, Chabert E (2006) Mechanical properties of high density polyurethane foams: I. effect of the density. *Composites Science and Technology* 66(15):2700–2708. <https://doi.org/10.1016/j.compscitech.2006.03.009>
34. Criscione JC, Humphrey JD, Douglas AS, Hunter WC (2000) An invariant basis for natural strain which yields orthogonal stress response terms in isotropic hyperelasticity. *J Mech Phys Solids* 48(12):2445–2465. [https://doi.org/10.1016/S0022-5096\(00\)00023-5](https://doi.org/10.1016/S0022-5096(00)00023-5)

Publisher's Note Springer Nature remains neutral with regard to jurisdictional claims in published maps and institutional affiliations.

Springer Nature or its licensor (e.g. a society or other partner) holds exclusive rights to this article under a publishing agreement with the author(s) or other rightsholder(s); author self-archiving of the accepted manuscript version of this article is solely governed by the terms of such publishing agreement and applicable law.